Biological Psychiatry

Archival Report

Strength of Excitatory Inputs to Layer 3 Pyramidal Neurons During Synaptic Pruning in the Monkey Prefrontal Cortex: Relevance for the Pathogenesis of Schizophrenia

Guillermo Gonzalez-Burgos, Takeaki Miyamae, Yosuke Nishihata, Olga L. Krimer, and David A. Lewis

ABSTRACT

BACKGROUND: In schizophrenia, layer 3 pyramidal neurons (L3PNs) of the dorsolateral prefrontal cortex exhibit deficits in markers of excitatory synaptic inputs that are thought to disrupt the patterns of neural network activity essential for cognitive function. These deficits are usually interpreted under Irwin Feinberg's hypothesis of altered synaptic pruning, which postulates that normal periadolescent pruning, thought to preferentially eliminate weak/immature synapses, is altered in schizophrenia. However, it remains unknown whether periadolescent pruning on L3PNs in the primate dorsolateral prefrontal cortex selectively eliminates weak excitatory synapses or uniformly eliminates excitatory synapses across the full distribution of synaptic strengths.

METHODS: To distinguish between these alternative models of synaptic pruning, we assessed the densities of dendritic spines, the site of most excitatory inputs to L3PNs, and the distributions of excitatory synaptic strengths in dorsolateral prefrontal cortex L3PNs from male and female monkeys across the periadolescent period of synaptic pruning. We used patch-clamp methods in acute brain slices to record miniature excitatory synaptic currents and intracellular filling with biocytin to quantify dendritic spines.

RESULTS: On L3PNs, dendritic spines exhibited the expected age-related decline in density, but mean synaptic strength and the shape of synaptic strength distributions remained stable with age.

CONCLUSIONS: The absence of age-related differences in mean synaptic strength and synaptic strength distributions supports the model of a uniform pattern of synaptic pruning across the full range of synaptic strengths. The implications of these findings for the pathogenesis and functional consequences of dendritic spine deficits in schizophrenia are discussed.

https://doi.org/10.1016/j.biopsych.2023.01.019

Cognitive deficits, among the most debilitating clinical features of schizophrenia, might reflect, at least in part, circuit dysfunction in the dorsolateral prefrontal cortex (DLPFC) (1). For example, in the DLPFC of individuals with schizophrenia, layer 3 pyramidal neurons (L3PNs) have a lower density of dendritic spines (2–4), the main site of excitatory input to PNs (5). These findings suggest that a reduced excitatory synaptic drive decreases the activity of L3PNs, disrupting the patterns of network activity essential for cognitive function (6).

The cause of lower spine density on L3PNs in schizophrenia remains unclear (7), but this deficit is frequently interpreted under Irwin Feinberg's influential synaptic pruning hypothesis (7,8), which has 2 key components. The first component posits that the protracted pruning of excitatory synapses normally observed between childhood and early adult life (9–11) is altered in schizophrenia (8). Unfortunately, this component of the hypothesis remains challenging to test directly in people with schizophrenia.

The second component posits that the pattern of normal excitatory synapse pruning during adolescence is similar to that observed during early cortical development (8), when pruning selectively eliminates weak/immature synapses (12). However, this component remains untested in the primate DLPFC; thus, it is possible that normal pruning during adolescence follows a uniform pattern in which synapses are eliminated proportionally across the full distribution of synaptic strengths, preserving the relative strengths across all excitatory inputs to each neuron, as in homeostatic synaptic scaling (13,14). These 2 patterns of pruning are likely to produce different functional outcomes. Indeed, recent computational models showed that the selective pruning of weak synapses improves the performance of recurrent neural networks on working memory tasks but at the expense of decreasing the networks' capacity to learn new tasks (15). Thus, a homeostatic uniform pruning pattern might be advantageous for preserving the networks' plastic capacity for learning.

SEE COMMENTARY ON PAGE 280

 ISSN: 0006-3223

Because selective pruning of weak synapses or uniform pruning across all synaptic strengths (Figure 1) are predicted to have very different effects on the functional maturation of cortical circuitry, determining which pattern characterizes pruning has important implications for understanding the causes and consequences of lower spine density on L3PNs in the DLPFC of people with schizophrenia. Consequently, in this study we evaluated the pattern of pruning of excitatory synaptic inputs to L3PNs in the macaque monkey DLPFC, a model system (11,16) that recapitulates the years-long trajectory of normal pruning present in human DLPFC (9,17). We combined patch-clamp methods, to measure synaptic strength via recording of excitatory synaptic currents, and biocytin cell filling, to quantify dendritic spine density, in L3PNs from the DLPFC of rhesus monkeys with a range of ages that span the period of adolescence-related synaptic pruning. We found that dendritic spine quantity on L3PNs showed the expected decline with age, but mean excitatory synaptic strength and the shape of synaptic strength distributions remained stable with age. Thus, these findings support a uniform pattern of pruning across excitatory synaptic strengths and not a selective elimination of weak synapses. The implications of these findings for understanding the pathogenesis and functional consequences of deficits in excitatory synapses on dendritic spines in schizophrenia are discussed.

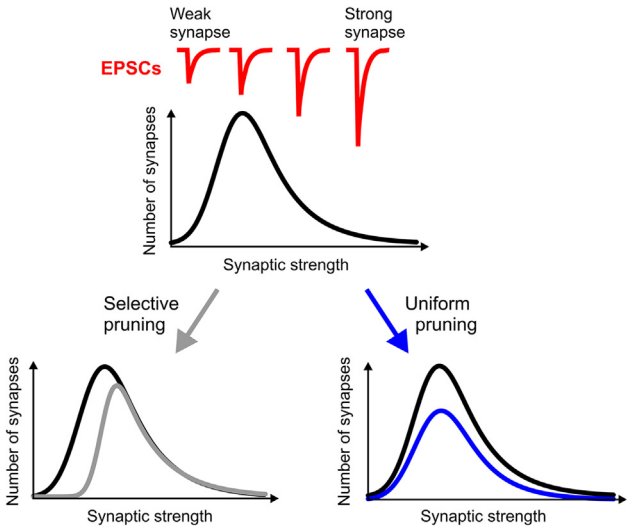

Figure 1. Schematic representation of the predicted effects for 2 alternative models of pruning on the distribution of synaptic strengths. (Top panel) The red traces represent excitatory postsynaptic currents (EPSCs) elicited at 4 example synapses ranging from weak to strong in strength. The black curve represents the histogram of distribution of synaptic strengths in a typical layer 3 pyramidal neuron before synaptic pruning occurs. (Left bottom panel) Curves of the synaptic strength distributions before synaptic pruning (black) and after selective pruning of weak synapses (gray). (Right bottom panel) Curves of the synaptic strength distributions before synaptic pruning (black) and after uniform pruning, proportional across the full distribution of synaptic strengths (blue). Whereas selective pruning increases the skewness of the distribution of synaptic strengths, uniform pruning does not change the shape of the distribution. For illustration purposes, selective pruning was modeled by deleting 30% of the synapses selectively from the bins with weaker synapses, leaving the bins with stronger synapses unchanged. To illustrate the uniform pruning model, we deleted 30% of the synapses in each bin of the distribution. Hence, the total number of synapses deleted to generate each scheme was identical, but different subsets of synapses were deleted.

METHODS AND MATERIALS

Animals and Surgical Procedures

All rhesus macaque monkeys ($N = 22$) in this study were used in a parallel study of the transcriptome of retrogradely-labeled L3PNs for which a fluorescent retrograde tracer was administered via intracortical injections in layer 3 of the right caudal DLPFC or left posterior parietal cortex (18). Following the tracer injections, animals received a systemic antibiotic (cefazolin 25 mg/kg, 2 times daily) and an analgesic (buprenorphine 0.01 mg/kg, 2 times daily) for 4 days. Two weeks after surgery, animals were euthanized (see below) using methods consistent with the American Veterinary Medical Association Guidelines for the Euthanasia of Animals, as previously described (19). We studied 3 groups of animals with mean ages across the protracted phase of pruning of excitatory axospinous synapses (10,11,16). At the time of the ex vivo electrophysiology experiments, the animals had mean ± SD ages of 1.6 ± 0.2 years ($n = 6$ animals), 3.2 ± 0.07 years ($n = 8$ animals), and 4.7 ± 0.1 years ($n = 8$ animals) with equal numbers of females and males per group. All housing and experimental procedures were conducted in accordance with United States Department of Agriculture and National Institutes of Health guidelines and were approved by the University of Pittsburgh Institutional Animal Care and Use Committee.

Brain Slice Preparation

Slices were prepared as described previously (19). Tissue blocks containing both banks of the rostral principal sulcus in the left DLPFC area 46 (in a location not containing L3PNs projecting to either of the injection sites) were obtained after the animals were deeply anesthetized and perfused transcardially (19) with ice-cold sucrose-modified artificial cerebrospinal fluid (ACSF) (mM): sucrose 200, NaCl 15, KCl 1.9, Na_2HPO_4 1.2, $NaHCO_3$ 33, $MgCl_2$ 6, $CaCl_2$ 0.5, glucose 10, and kynurenic acid 2; pH 7.3–7.4 when bubbled with 95% O_2/5% CO_2. Using the same ice-cold sucrose-modified ACSF, 300-μm-thick coronal slices were cut in a vibrating microtome (VT1000S; Leica Microsystems). Immediately after cutting, the slices were transferred to an incubation chamber at room temperature filled with standard ACSF (mM): NaCl 125, KCl 2.5, Na_2HPO_4 1.25, glucose 10, $NaHCO_3$ 25, $MgCl_2$ 1, and $CaCl_2$ 2; pH 7.3–7.4 when bubbled with 95% O_2/5% CO_2. All chemicals were purchased from Sigma-Aldrich.

Recording and Analysis of Spontaneous Miniature Excitatory Postsynaptic Currents

Between 1 and 14 hours after tissue slicing was completed, the slices were transferred to the recording chamber and superfused at 2 to 3 mL/minute with standard ACSF containing 10 μM gabazine and 1 μM tetrodotoxin but not kynurenic acid; bubbled with 95% O_2/5% CO_2 at 30 °C to 32 °C. Miniature excitatory postsynaptic currents (mEPSCs) were recorded from L3PNs identified visually by infrared differential interference contrast video microscopy using Olympus BX51 or Zeiss Axioskop FS2 microscopes and charge-coupled device video cameras (EXi Aqua, Q-Imaging). The L3PNs targeted for

recording were in the dorsal or ventral bank of the principal sulcus in DLPFC area 46 (Figure 2A). Voltage-clamp recordings were obtained, without series resistance compensation, using Multiclamp 700A or 700B amplifiers (Axon Instruments). Recordings were included in data analysis only if the resting membrane potential was ≤ -60 mV. All the neurons included in this study exhibited pyramidal morphology of soma and apical dendrite (Figure 2A). Recording pipettes had a resistance of 3 MΩ to 5 MΩ when filled with the following solution (mM): CsGluconate 120, NaCl 10, EGTA 0.2, HEPES 10, MgATP 4, NaGTP 0.3, NaPhosphocreatine 14, and biocytin 0.4%. The pH (7.2–7.3) was adjusted with CsOH. The series resistance (Rs) and membrane properties were monitored throughout the experiment using a voltage step (50 ms, 5 mV) delivered near the onset of each sweep. The Rs was measured offline using Signal scripts (20), and recordings were excluded from the analysis if the initial Rs was >15 MΩ or the Rs changed by >15% during the recordings (20). The mEPSCs were recorded while holding the L3PNs at a membrane potential of −80 mV. The mEPSCs were detected and analyzed using Mini Analysis software (Synaptosoft), starting ∼1 minute after the beginning of whole-cell recordings (20). All detected mEPSCs were inspected visually and were used to estimate the peak mEPSC amplitude. For additional details and methods for estimating synaptic conductance, see the Supplement.

Analysis of Dendritic Spine Quantity in Biocytin-Filled L3PNs

Histological processing of the slices containing biocytin-filled L3PNs was performed as described previously (19) (for details, see the Supplement). For each L3PN, a single primary basal dendrite was selected randomly and confirmed to have a natural ending within the thickness of the tissue section (i.e., the basal dendrite was not sectioned during slicing). On these dendrites, using differential interference contrast with a 63× objective, dendritic spines were identified throughout the length of a basal dendrite branch (Figure 2B). The reconstructed dendrite was examined using the Sholl Analysis menu in Neurolucida (increment radius 10 μm). The peak and mean spine densities were the maximum and average spine density values across Sholl compartments, respectively. Measurements of spine density in 2 different dendrites per L3PN were highly consistent (Figure S1).

Statistical Analysis

The data are shown as mean ± SD. The effects of age and sex were determined using linear mixed effects model or Student's *t* test, after running the Shapiro-Wilk and D'Agostino's K^2 normality tests on the residuals of the data. If normality of distribution was rejected, we used logarithm transformation (Table S1).

RESULTS

Biocytin-Filled L3PNs Show Significant Pruning of Dendritic Spines Across the Periadolescence Period

We reconstructed the dendritic tree (Figure 2A) of a random sample of the L3PNs filled with biocytin in female and male monkeys from each of the 3 age groups. Dendritic spines (Figure 2B) were traced throughout the length of a single basal dendrite per L3PN (Figure 2C); basal dendrites have been shown to capture the time course and magnitude of pruning observed throughout the dendritic tree of L3PNs (16).

Spine density differed markedly across the length of each dendrite, increasing from zero near the soma to a peak near the mid portion and declining toward the distal end (Figure 2C). Both peak (Figure 2D) and mean (Figure 2E) spine densities were similar in L3PNs from the 1.6- and 3.2-year-old groups and significantly lower in the 4.7-year-old group. Neither peak ($F_{1,34} = 2.613$, $p = .115$) nor mean ($F_{1,34} = 0.136$, $p = .716$) spine densities differed between sexes.

The length of single basal dendrites did not differ between age groups (1.6-year-old, 228 ± 38 μm, $n = 16$; 3.2-year-old, 224 ± 25 μm, $n = 12$; and 4.7-year-old, 231 ± 40 μm, $n = 12$; $F_{2,6.9} = 0.145$, $p = .867$), consistent with prior reports that dendritic length does not differ across postnatal development in these neurons (16,21,22). Given constant dendrite length across age groups, the lower spine density per basal dendrite in L3PNs from the 4.7-year-old animals resulted in ∼30% lower total number of spines per basal dendrite in those animals than in those from the 2 younger groups (Figure 2F). The differences in spine number by age were most prominent in the middle dendrite compartments, negligible in the proximal dendrite, and small in the distal dendrite (Figure 2G).

The Distribution of Excitatory Synaptic Strengths Remains Stable Across the Periadolescence Period

To study the distribution of excitatory synaptic strengths in L3PNs across the synaptic pruning period, we recorded mEPSCs. Each mEPSC represents the quantal current elicited at a single synapse; hence, the distribution of mEPSC amplitudes for a given neuron estimates the distribution of synaptic strengths across that neuron's population of glutamate synapses (13). The shape of the distribution of mEPSC amplitudes should differ by age based on the synaptic pruning pattern, shifting to the right with selective pruning of weak synapses but remaining stable if synaptic pruning follows a uniform pattern. We tested these predictions comparing the distributions of mEPSC amplitudes in L3PNs from the 3 age groups.

In all L3PNs from all age groups, the mEPSCs showed fast decay kinetics (Figure 3A) consistent with being primarily mediated by AMPA receptors, as expected from recording at a holding potential of −80 mV with 1 mM extracellular Mg^{2+}. The cumulative probability distributions of mEPSC amplitudes (Figure 3B) were positively skewed, with a high proportion of mEPSCs in the smaller amplitude range (Figure 3B insets). However, the shape of the distributions had substantial cell-to-cell variability in all age groups (Figure 3B). Hence, we estimated the skewness (Figure 3C) and coefficient of variation (Figure 3D) to assess any group differences in the shape of the distributions.

The skewness of the distributions did not differ significantly across age groups (Figure 3C), whereas the coefficient of variation increased slightly but nonsignificantly (Figure 3D). The small differences in the coefficient of variation (Figure 3D) could reflect the presence of a small subset of L3PNs with a greater proportion of larger mEPSCs and thus a rightward shift

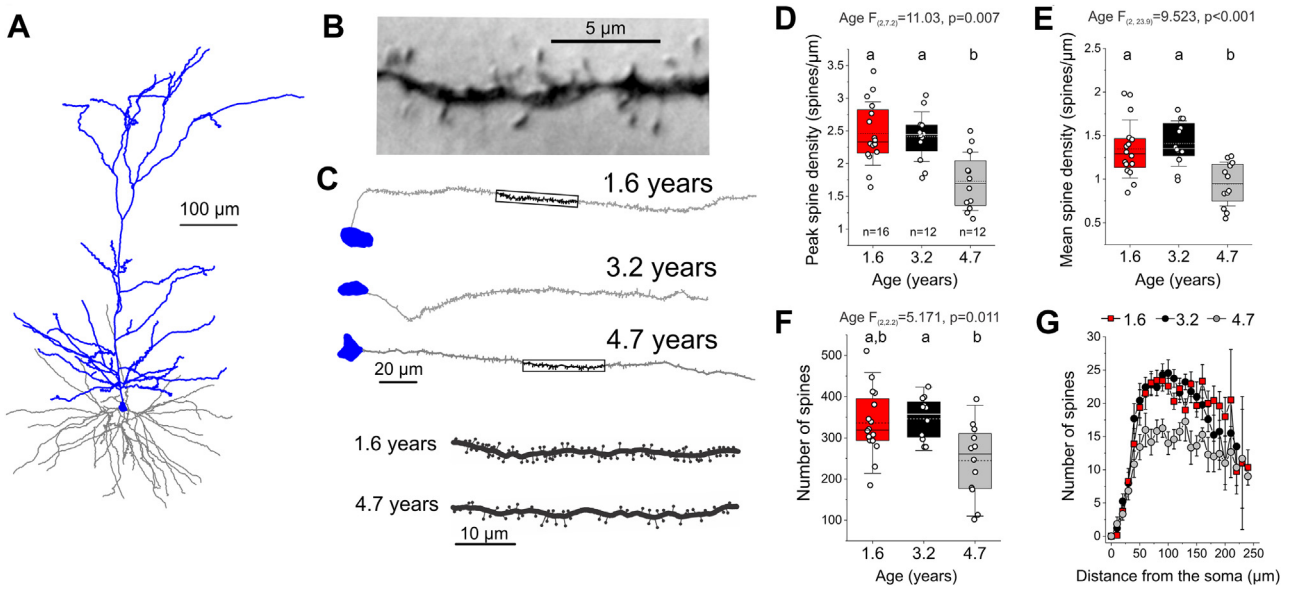

Figure 2. Dendritic spine quantification in basal dendrites of biocytin-filled layer 3 pyramidal neurons. **(A)** Reconstruction of a representative layer 3 pyramidal neuron dendritic tree (apical dendrite and soma: blue; basal dendrite: gray). **(B)** Differential interference contrast image of a segment of dendrite in which spines were quantified. **(C)** Examples of basal dendrites with dendritic spines that were quantified between the soma and distal end. The rectangles indicate the segments of dendrites shown at higher magnification at the bottom. **(D–F)** Peak density, mean density, and absolute number of basal dendritic spines, respectively, for layer 3 pyramidal neurons in the 3 age groups. Shown here, and in all other box plots, are the mean (dashed line), median (solid line), and SD. Groups with different letters were significantly different in post hoc contrasts with Tukey's correction ($p < .02$). **(G)** Number of spines in basal dendrites as a function of distance from the soma.

in the distribution consistent with selective elimination of weak synapses on those neurons. However, the abundance of L3PNs with either low or high skewness values in their distributions did not differ between age groups (Figure 3E). Finally, the kurtosis parameter, which measures the shape of a distribution around its tails, did not differ between groups (Figure S2). These analyses of the distributions of synaptic strengths suggest that synapses on L3PNs from monkey DLPFC are eliminated proportionally throughout the full distribution of synaptic strengths, consistent with a uniform pattern of synaptic pruning (Figure 1).

The Average Strength of Excitatory Synapses Remains Stable Across the Periadolescence Period

The analysis of the single-cell distributions (Figure 3) suggests that the average mEPSC amplitude, which measures the contribution per synapse to the total excitatory drive per neuron, does not differ by age. The average mEPSC amplitudes largely overlapped between age groups (Figure 4A), showing small (≤1.45 pA), albeit significant ($F_{2,11.1} = 4.681$, $p = .034$), differences between group means. Data plots from individual animals did not show any apparent clustering of the data by animal (Figure 4B), suggesting that the small age-related differences in average mEPSC amplitude were not due to within-animal data correlations (23). Furthermore, the presence of lower values in the 3.2-year-old group relative to both the 1.6-year-old (−9.1%) and 4.7-year-old (−10.5%) groups does not support a consistent difference with age. To further test for differences in average mEPSC amplitude that may be associated with the age-related differences in dendritic spine quantities, we computed the average mEPSC amplitude after combining the 1.6- and 3.2-year-old groups (12.5 ± 2.7 pA, $n = 142$), which did not differ in spine number, and compared it with the value from 4.7-year-old group (13.4 ± 3.4 pA, $n = 77$), which had a 30% lower spine number. The small differences in mEPSC amplitude (∼0.9 pA) between these age groups were not significant ($F_{1,5.2} = 0.773$, $p = .418$), suggesting that the peak excitatory conductance does not differ in a manner temporally associated with the age-related differences in dendritic spine quantities (Figure 2).

Next, we estimated the differences in excitatory drive associated with the age-related differences in dendritic spine quantity. Given the lack of differences in mEPSC amplitude (Figures 3 and 4), differences in excitatory drive must be due solely to differences in the quantity of axospinous synapses (Figure 2). To evaluate the magnitude of the age-related differences in excitatory drive per L3PN, we estimated the total excitatory postsynaptic conductance (EPSG) in basal dendrites using our measures of dendritic spines and mean mEPSC amplitude. Because the shape of the distributions of mEPSC amplitude did not differ between age groups, the mean mEPSC amplitude is a good estimator of the average synapse strength across age groups. Although our goal was estimating EPSG in the full sample of L3PNs, dendritic spines were quantified only in a subset of the L3PNs (Figure 2). Hence, this subset was first used to determine whether, for estimating the EPSG, the average spine number of each age group is an acceptable proxy of the actual spine number in each L3PN. The average single-synapse conductance, or peak miniature EPSG, was estimated using each neuron's average peak mEPSC amplitude. Across L3PNs in each age

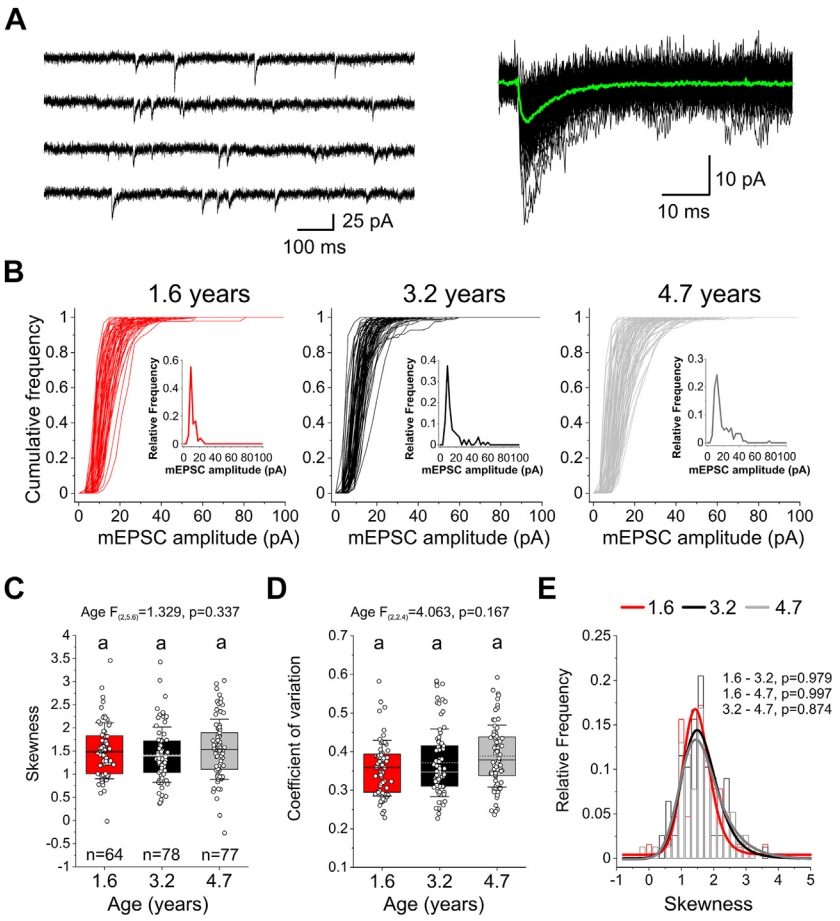

Figure 3. Distributions of miniature excitatory synaptic current (mEPSC) amplitude in layer 3 pyramidal neurons from 1.6-, 3.2-, and 4.7-year-old animals. **(A)** Left panel, example traces of voltage-clamp recordings at −80 mV holding potential showing mEPSCs recorded from a layer 3 pyramidal neuron. Right panel, multiple mEPSCs superimposed together with their average waveform (green). **(B)** Single-cell cumulative probability distributions. Insets: relative frequency of mEPSC amplitudes for an example layer 3 pyramidal neuron in each age group. **(C)** Box plots of the skewness parameter. Groups sharing the same letter were not significantly different in post hoc contrasts with Tukey's correction ($p > .243$). **(D)** Box plots of coefficient of variation. Groups sharing the same letter were not significantly different in post hoc contrasts with Tukey's correction ($p > .627$). **(E)** Relative frequency of the skewness parameter values. Shown are the results of comparisons using the Kolmogorov-Smirnov tests for difference between distributions.

group, our estimates of miniature EPSG (1.6-year-old: 193 ± 41 pS; 3.2-year-old: 151 ± 33 pS; and 4.7-year-old: 184 ± 67 pS) were well within the range predicted by biophysically realistic models of monkey L3PNs (24). The EPSG estimated using the actual number of dendritic spines per L3PN (Figure 4C) or the average spine number of the age group (Figure 4D) were very similar and significantly correlated (Pearson's $r = 0.679$, $p = 2.8 \times 10^{-6}$). Having verified that the average spine number of the age group is an acceptable proxy, we estimated the EPSG in the full sample of L3PNs. We found significant differences by age (Figure 4E) with the EPSG ~22% and ~29% lower in L3PNs from the 4.7-year-old group than in the 1.6- and 3.2-year-old groups, respectively (Figure 4E). Estimates of spine quantities in basal dendrites adequately capture the effects of synaptic pruning throughout the L3PN dendritic tree (16). Therefore, our results suggest that the magnitude of the excitatory synaptic conductance available to be recruited in each L3PN is significantly lower after pruning, although our experiments cannot predict what fraction of the total excitatory conductance available is actually recruited because the excitatory drive to each neuron fluctuates in vivo.

Recordings of EPSCs with somatic voltage clamp are subject to space-clamp errors that affect the EPSG estimates (25). However, dendritic length, an important determinant of space-clamp errors, does not differ across development in DLPFC L3PNs (16,21,22). Moreover, mEPSCs with slower rising phase slope (Figure 5A), presumably originating distally and thus subject to greater space-clamp errors (25–27), had similar amplitude (Figure 5B) and distribution across age groups (Figure 5C), suggesting similar space-clamp errors.

Finally, the mEPSC frequency varied largely from cell to cell, as in other studies (14,28), was not correlated with spine quantity, and did not differ between age groups (Figure S3).

DISCUSSION

We assessed dendritic spine density and the distribution of excitatory synaptic strengths in L3PNs from monkey DLPFC across the synaptic pruning period. While finding the expected age-related decline in dendritic spines, we did not find differences by age in the shape of the synaptic strength distributions or the average synaptic strength. These findings support the uniform model of excitatory synaptic pruning and not the selective elimination of weak/immature synapses. Below, we discuss the strengths of this study and the implications of

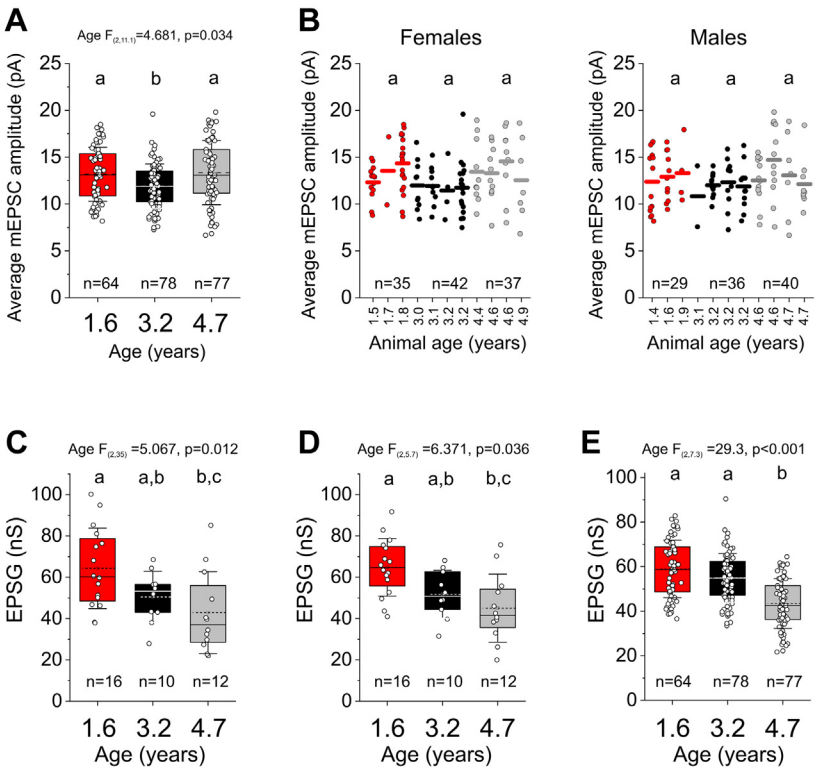

Figure 4. Estimates of the average excitatory synaptic strength and excitatory synaptic conductance in basal dendrites. **(A)** The miniature excitatory synaptic current (mEPSC) amplitude was averaged across all mEPSCs detected in single layer 3 pyramidal neurons (L3PNs) and compared between age groups. Groups labeled with different letters were significantly different in post hoc contrasts with Tukey's correction ($p < .04$). **(B)** Plots of average mEPSC for individual animals in each age group. Groups labeled with the same letter did not differ in post hoc contrasts with Tukey's correction ($p > .109$). **(C)** Estimates of the excitatory postsynaptic conductance (EPSG) per basal dendrite using the miniature EPSG estimate and the actual number of spines quantified in each L3PN. Groups labeled with the same letter did not differ in post hoc contrasts with Tukey's correction ($p > .385$). **(D)** Estimates of the EPSG obtained using the miniature EPSG estimate and the average number of spines per basal dendrite for each age group, from the same groups of L3PNs as in **(C)**. Groups labeled with the same letter did not differ in post hoc contrasts with Tukey's correction ($p > .101$). **(E)** The EPSG was estimated for all L3PNs in each age group using the miniature EPSG estimate for each L3PN and the average number of spines per basal dendrite for the age group. Groups labeled with different letters were significantly different in post hoc contrasts with Tukey's correction ($p < .001$).

these results for understanding the nature of protracted synaptic pruning and of dendritic spine deficits in schizophrenia.

Robustness of the Findings of This Study

The robustness of the findings of this study, the first to assess excitatory synaptic strength in L3PNs from primate DLPFC during the periadolescence period, is supported by various lines of evidence. First, our finding that dendritic spine quantity in biocytin-filled DLPFC L3PNs declines during periadolescence is consistent with the previous developmental studies using Golgi impregnation to assess spine density in monkey DLPFC L3PNs (16) or electron microscopy to quantify axospinous synapse density in layer 3 of monkey DLPFC (10,11) but with a time course that differs from that reported for PFC area 12v (29). Second, our results, which do not indicate selective pruning of weak/immature synapses during adolescence, are supported by our findings in a different cohort of monkeys that most glutamate synapses on monkey DLPFC L3PNs reach the adult level of maturation before the period of protracted synaptic pruning (30). Third, our findings of a stable distribution of synaptic strengths across age groups is consistent with the absence of developmental shifts in messenger RNA levels of key ionotropic glutamate receptor subunit genes in monkey DLPFC L3PNs across adolescence (31,32). Fourth, our use of both female and male animals in each age group insures that our findings are not biased by sex, and the absence of differences by sex is consistent with prior studies of spine density across postnatal development in macaque monkeys (16). Fifth, our estimates of mEPSC amplitude are highly similar to those reported by another research group for L3PNs from the DLPFC of adult monkeys (33). Finally, the use of a nonhuman primate model system is important for the study of the synaptic pruning hypothesis of schizophrenia, given that periadolescent synaptic pruning is consistently observed in both monkey (10,11,16) and human (9,17) DLPFC, whereas studies of rodent PFC have reported mixed results (34–40), possibly due to regional and/or species differences.

Implications for Understanding the Role of Protracted Synaptic Pruning in DLPFC Maturation

A key component of Feinberg's original synaptic pruning hypothesis is that normal periadolescent pruning "may be analogous to the programmed elimination of neural elements in very early development" (8). During early development weak/immature synapses are thought to be preferentially eliminated (12), hence, Feinberg's initial postulate implies that weak/immature synapses are abundant at the onset of synaptic pruning but represent a smaller proportion of excitatory synapses when pruning is complete.

Because no previous studies had tested whether the fractions of weak and/or strong synapses in DLPFC L3PNs differ after synaptic pruning, we studied the distribution of excitatory synaptic strengths in these neurons during the periadolescence period. We found that the distributions of mEPSC amplitudes in DLPFC L3PNs do not differ by age, hence contradicting the selective elimination of weak/immature synapses but supporting a uniform pattern of excitatory synaptic

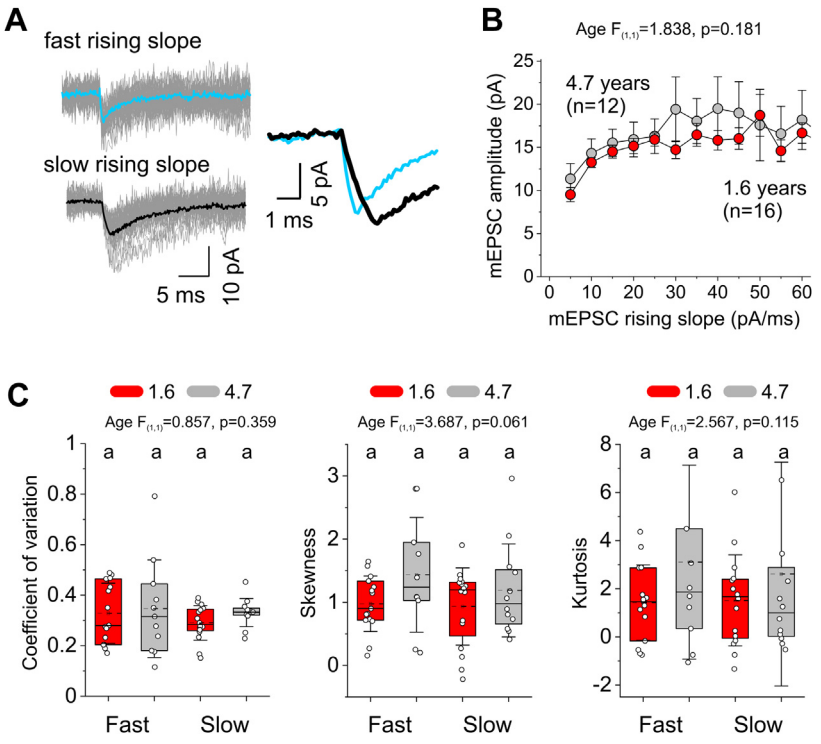

Figure 5. Comparison of the miniature excitatory synaptic current (mEPSC) amplitude for mEPSCs sorted as a function of the slope of their rising phase. **(A)** Left panel, examples of mEPSCs with fast rising phase slope, the individual mEPSCs are shown aligned and superimposed (gray traces) together with their average (fast rising in blue, slow rising in black). Right panel, the average mEPSCs with slow and fast rising phase slope are shown superimposed to compare the time course of the rising phase. **(B)** Plot of mEPSC amplitude as a function of rising phase slope. Here and in **(C)**, we compared after sorting by their rising phase slope, the mEPSCs recorded from layer 3 pyramidal neurons of the 1.6- (n = 16) and 4.7-year-old (n = 16) groups in which dendritic spines were quantified (Figure 2). **(C)** Bar graphs depict the coefficient of variation, skewness, and kurtosis for the amplitude of mEPSCs with slow (<20 pA/ms) or fast (>30 pA/ms) rising phase slopes. Groups labeled with the same letter did not differ in post hoc contrasts with Tukey's correction (coefficient of variation, $p > .608$; skewness, $p > .253$; and kurtosis, $p > .549$).

pruning across the full range of synaptic strengths. This interpretation is consistent with the only prior study of synaptic maturation in monkey DLPFC L3PNs, which suggested that excitatory synapses on L3PNs mature pre- and postsynaptically before synaptic pruning begins (30). The significant fraction of weak synapses observed in L3PNs may play important functional roles, including allowing broader representations of certain stimuli. However, our current and prior findings (30) suggest that the abundance of weak/immature synapses, especially of the NMDA-only silent class (41), does not change during the pruning period. Thus it seems unlikely that the functional roles of weak synapses are refined via periadolescent synaptic pruning. Importantly, although we only studied the AMPA receptor–mediated component of mEPSCs, findings from previous experiments (30) suggest similar results vis-à-vis the NMDA receptor–mediated component (Supplemental Discussion).

Importantly, age did not significantly affect the mEPSC frequency, a dynamic parameter that could be associated with the number of synapses per cell but is highly dependent on the glutamate release probability. In monkey DLPFC, the release probability displays large cell-to-cell variability and does not change with the reduction in synapse number during periadolescent development (30).

Working memory function, and the associated DLPFC neuron activity, improve during the periadolescence period (42,43), but the role of synaptic pruning in these developmental changes remains unclear. The developmental improvements in working memory function have been modeled in recurrent neural networks (15,44), and results indicated that selectively pruning a large fraction of weak synapses improved performance on a particular working memory task but at the cost of reducing performance on other tasks (15). In other studies, reducing the total number of synaptic connections without selectively eliminating weak synapses increased the computational efficiency and performance of complex networks (45). Therefore, uniform synaptic pruning in DLPFC L3PNs could improve working memory developmentally by eliminating synapses while preserving the distribution of synaptic strengths, thus having a homeostatic synaptic scaling–like effect (46) while avoiding some of the costs associated with selectively pruning weak synapses.

Importantly, because we were not able to study mEPSCs longitudinally, we could not determine whether the synaptic strength distributions remain stable through the periadolescence period as a consequence of a pruning process that precisely sculpts those distributions. Changes in network activity through the periadolescence period may trigger homeostatic plasticity mechanisms that adjust the distribution of synaptic weights (46). Despite the significant quantity of synapses pruned, single-neuron activity in the DLPFC during working memory tasks increases during periadolescent development (43,47,48), suggesting that homeostatic mechanisms likely play a complex role (see Supplemental Discussion).

Implications for Understanding the Nature of Dendritic Spine Deficits in Schizophrenia

The idea that the normal pattern of periadolescent pruning in L3PNs is uniform, eliminating synapses proportionally across the full distribution of excitatory synaptic strengths and without selectively eliminating weak synapses (Figure 1), may

have several implications for understanding the origin and consequences of synaptic deficits in schizophrenia. For example, studies of the layer 3 neuropil of the primary auditory cortex showed lower spine density in schizophrenia (49) principally due to fewer small spines (50,51). Because small spines typically have small spine heads that receive weaker excitatory synapses (33,52–54), these findings suggest a selective deficit of weaker synapses in schizophrenia. Moreover, these results, in concert with the present findings, suggest that the synaptic pruning process in schizophrenia might be abnormal, selectively eliminating normal numbers of strong synapses but eliminating an excess of weak synapses, thus altering the normal distribution of synaptic strengths (Supplemental Discussion).

The current study is, to our knowledge, the first to show, by estimating the EPSG in basal dendrites, that the excitatory drive available for recruitment decreases with normal synaptic pruning, supporting the idea that the synaptic deficits in schizophrenia, whether due to exaggerated pruning and/or deficient synaptogenesis (55), decrease the excitatory drive to L3PNs (6). Moreover, if as reported for auditory cortex neuropil (50,51), DLPFC L3PNs have fewer small spines in schizophrenia, then these neurons may have both reduced excitatory drive and an altered distribution of excitatory synaptic strengths, disrupting the processing of working memory–related information.

ACKNOWLEDGMENTS AND DISCLOSURES

This work was supported by the National Institute of Mental Health (Grant No. MH 051234 [to DAL]).

We thank Samuel Dienel and Kate Gurnsey for excellent assistance during surgical procedures.

DAL receives research funding from Merck. All other authors report no biomedical financial interests or potential conflicts of interest.

ARTICLE INFORMATION

From the Translational Neuroscience Program, Department of Psychiatry, University of Pittsburgh School of Medicine, Pittsburgh, Pennsylvania (GG-B, TM, YN, OLK, DAL).

YN is currently affiliated with the Department of Psychiatry, Nara Medical University School of Medicine, Kashihara, Japan.

Address correspondence to Guillermo Gonzalez-Burgos, Ph.D., at gburgos@pitt.edu, or David A. Lewis, M.D., at lewisda@upmc.edu.

Received Oct 10, 2022; revised Jan 6, 2023; accepted Jan 23, 2023.

Supplementary material cited in this article is available online at https://doi.org/10.1016/j.biopsych.2023.01.019.

REFERENCES

1. Smucny J, Dienel SJ, Lewis DA, Carter CS (2022): Mechanisms underlying dorsolateral prefrontal cortex contributions to cognitive dysfunction in schizophrenia. Neuropsychopharmacology 47:292–308.
2. Garey LJ, Ong WY, Patel TS, Kanani M, Davis A, Mortimer AM, *et al.* (1998): Reduced dendritic spine density on cerebral cortical pyramidal neurons in schizophrenia. J Neurol Neurosurg Psychiatry 65:446–453.
3. Glantz LA, Lewis DA (2000): Decreased dendritic spine density on prefrontal cortical pyramidal neurons in schizophrenia. Arch Gen Psychiatry 57:65–73.
4. Konopaske GT, Lange N, Coyle JT, Benes FM (2014): Prefrontal cortical dendritic spine pathology in schizophrenia and bipolar disorder. JAMA Psychiatry 71:1323–1331.
5. DeFelipe J, Fariñas I (1992): The pyramidal neuron of the cerebral cortex: Morphological and chemical characteristics of the synaptic inputs. Prog Neurobiol 39:563–607.
6. Lewis DA, Curley AA, Glausier JR, Volk DW (2012): Cortical parvalbumin interneurons and cognitive dysfunction in schizophrenia. Trends Neurosci 35:57–67.
7. Johnson MB, Hyman SE (2022): A critical perspective on the synaptic pruning hypothesis of schizophrenia pathogenesis. Biol Psychiatry 92:440–442.
8. Feinberg I (1982): Schizophrenia: Caused by a fault in programmed synaptic elimination during adolescence? J Psychiatr Res 17:319–334.
9. Huttenlocher PR (1979): Synaptic density in human frontal cortex - Developmental changes and effects of aging. Brain Res 163:195–205.
10. Rakic P, Bourgeois JP, Eckenhoff MF, Zecevic N, Goldman-Rakic PS (1986): Concurrent overproduction of synapses in diverse regions of the primate cerebral cortex. Science 232:232–235.
11. Bourgeois JP, Goldman-Rakic PS, Rakic P (1994): Synaptogenesis in the prefrontal cortex of rhesus monkeys. Cereb Cortex 4:78–96.
12. Faust TE, Gunner G, Schafer DP (2021): Mechanisms governing activity-dependent synaptic pruning in the developing mammalian CNS. Nat Rev Neurosci 22:657–673.
13. Turrigiano GG, Nelson SB (2004): Homeostatic plasticity in the developing nervous system. Nat Rev Neurosci 5:97–107.
14. Wen W, Turrigiano GG (2021): Developmental regulation of homeostatic plasticity in mouse primary visual cortex. J Neurosci 41:9891–9905.
15. Averbeck BB (2022): Pruning recurrent neural networks replicates adolescent changes in working memory and reinforcement learning. Proc Natl Acad Sci USA 119:e2121331119.
16. Anderson SA, Classey JD, Condé F, Lund JS, Lewis DA (1995): Synchronous development of pyramidal neuron dendritic spines and parvalbumin-immunoreactive chandelier neuron axon terminals in layer III of monkey prefrontal cortex. Neuroscience 67:7–22.
17. Petanjek Z, Judaš M, Šimic G, Rasin MR, Uylings HB, Rakic P, Kostovic I (2011): Extraordinary neoteny of synaptic spines in the human prefrontal cortex. Proc Natl Acad Sci USA 108:13281–13286.
18. Arion D, Enwright JF, Gonzalez-Burgos G, Lewis DA (2023): Differential gene expression between callosal and ipsilateral projection neurons in the monkey dorsolateral prefrontal and posterior parietal cortices. Cereb Cortex 33:1581–1594.
19. González-Burgos G, Miyamae T, Krimer Y, Gulchina Y, Pafundo DE, Krimer O, *et al.* (2019): Distinct properties of layer 3 pyramidal neurons from prefrontal and parietal areas of the monkey neocortex. J Neurosci 39:7277–7290.
20. Miyamae T, Chen K, Lewis DA, Gonzalez-Burgos G (2017): Distinct physiological maturation of parvalbumin-positive neuron subtypes in mouse prefrontal cortex. J Neurosci 37:4883–4902.
21. Lambe EK, Krimer LS, Goldman-Rakic PS (2000): Differential postnatal development of catecholamine and serotonin inputs to identified neurons in prefrontal cortex of rhesus monkey. J Neurosci 20:8780–8787.
22. Gonzalez-Burgos G, Miyamae T, Pafundo DE, Yoshino H, Rotaru DC, Hoftman G, *et al.* (2015): Functional maturation of GABA synapses during postnatal development of the monkey dorsolateral prefrontal cortex. Cereb Cortex 25:4076–4093.
23. Yu Z, Guindani M, Grieco SF, Chen L, Holmes TC, Xu X (2022): Beyond t test and ANOVA: Applications of mixed-effects models for more rigorous statistical analysis in neuroscience research. Neuron 110:21–35.
24. Amatrudo JM, Weaver CM, Crimins JL, Hof PR, Rosene DL, Luebke JI (2012): Influence of highly distinctive structural properties on the excitability of pyramidal neurons in monkey visual and prefrontal cortices. J Neurosci 32:13644–13660.
25. Williams SR, Mitchell SJ (2008): Direct measurement of somatic voltage clamp errors in central neurons. Nat Neurosci 11:790–798.
26. Spruston N, Jaffe DB, Williams SH, Johnston D (1993): Voltage- and space-clamp errors associated with the measurement of electrotonically remote synaptic events. J Neurophysiol 70:781–802.

27. Henze DA, Cameron WE, Barrionuevo G (1996): Dendritic morphology and its effects on the amplitude and rise-time of synaptic signals in hippocampal CA3 pyramidal cells. J Comp Neurol 369:331–344.
28. Wu CH, Ramos R, Katz DB, Turrigiano GG (2021): Homeostatic synaptic scaling establishes the specificity of an associative memory. Curr Biol 31:2274–2285.e5.
29. Elston GN, Oga T, Fujita I (2009): Spinogenesis and pruning scales across functional hierarchies. J Neurosci 29:3271–3275.
30. Gonzalez-Burgos G, Kroener S, Zaitsev AV, Povysheva NV, Krimer LS, Barrionuevo G, Lewis DA (2008): Functional maturation of excitatory synapses in layer 3 pyramidal neurons during postnatal development of the primate prefrontal cortex. Cereb Cortex 18:626–637.
31. Liu X, Somel M, Tang L, Yan Z, Jiang X, Guo S, *et al.* (2012): Extension of cortical synaptic development distinguishes humans from chimpanzees and macaques. Genome Res 22:611–622.
32. Datta D, Arion D, Lewis DA (2015): Developmental expression patterns of GABAA receptor subunits in layer 3 and 5 pyramidal cells of monkey prefrontal cortex. Cereb Cortex 25:2295–2305.
33. Medalla M, Luebke JI (2015): Diversity of glutamatergic synaptic strength in lateral prefrontal versus primary visual cortices in the rhesus monkey. J Neurosci 35:112–127.
34. Drzewiecki CM, Willing J, Juraska JM (2016): Synaptic number changes in the medial prefrontal cortex across adolescence in male and female rats: A role for pubertal onset. Synapse 70:361–368.
35. Boivin JR, Piekarski DJ, Thomas AW, Wilbrecht L (2018): Adolescent pruning and stabilization of dendritic spines on cortical layer 5 pyramidal neurons do not depend on gonadal hormones. Dev Cogn Neurosci 30:100–107.
36. Delevich K, Okada NJ, Rahane A, Zhang Z, Hall CD, Wilbrecht L (2020): Sex and pubertal status influence dendritic spine density on frontal corticostriatal projection neurons in mice. Cereb Cortex 30:3543–3557.
37. Mallya AP, Wang HD, Lee HNR, Deutch AY (2019): Microglial pruning of synapses in the prefrontal cortex during adolescence. Cereb Cortex 29:1634–1643.
38. Markham JA, Mullins SE, Koenig JI (2013): Periadolescent maturation of the prefrontal cortex is sex-specific and is disrupted by prenatal stress. J Comp Neurol 521:1828–1843.
39. Yilmaz M, Yalcin E, Presumey J, Aw E, Ma M, Whelan CW, *et al.* (2021): Overexpression of schizophrenia susceptibility factor human complement C4A promotes excessive synaptic loss and behavioral changes in mice. Nat Neurosci 24:214–224.
40. Schalbetter SM, von Arx AS, Cruz-Ochoa N, Dawson K, Ivanov A, Mueller FS, *et al.* (2022): Adolescence is a sensitive period for prefrontal microglia to act on cognitive development. Sci Adv 8: eabi6672.
41. Vardalaki D, Chung K, Harnett MT (2022): Filopodia are a structural substrate for silent synapses in adult neocortex. Nature 612:323–327.
42. Constantinidis C, Luna B (2019): Neural substrates of inhibitory control maturation in adolescence. Trends Neurosci 42:604–616.
43. Zhou X, Zhu D, Qi XL, Li S, King SG, Salinas E, *et al.* (2016): Neural correlates of working memory development in adolescent primates. Nat Commun 7:13423.
44. Liu YH, Zhu J, Constantinidis C, Zhou X (2021): Emergence of prefrontal neuron maturation properties by training recurrent neural networks in cognitive tasks. iScience 24:103178.
45. Hassibi B, Stork D (1993): Second order derivatives for network pruning: Optimal brain surgeon. In: Hanson S, Cowan J, Giles C, editors. Advances in Neural Information Processing Systems. Vancouver: Morgan Kaufmann Publishers, 164–171.
46. Turrigiano GG (2008): The self-tuning neuron: Synaptic scaling of excitatory synapses. Cell 135:422–435.
47. Zhou X, Zhu D, Qi XL, Lees CJ, Bennett AJ, Salinas E, *et al.* (2013): Working memory performance and neural activity in prefrontal cortex of peripubertal monkeys. J Neurophysiol 110:2648–2660.
48. Zhou X, Zhu D, Katsuki F, Qi XL, Lees CJ, Bennett AJ, *et al.* (2014): Age-dependent changes in prefrontal intrinsic connectivity. Proc Natl Acad Sci USA 111:3853–3858.
49. Sweet RA, Henteleff RA, Zhang W, Sampson AR, Lewis DA (2009): Reduced dendritic spine density in auditory cortex of subjects with schizophrenia. Neuropsychopharmacology 34:374–389.
50. MacDonald ML, Alhassan J, Newman JT, Richard M, Gu H, Kelly RM, *et al.* (2017): Selective loss of smaller spines in schizophrenia. Am J Psychiatry 174:586–594.
51. McKinney BC, MacDonald ML, Newman JT, Shelton MA, DeGiosio RA, Kelly RM, *et al.* (2019): Density of small dendritic spines and microtubule-associated-protein-2 immunoreactivity in the primary auditory cortex of subjects with schizophrenia. Neuropsychopharmacology 44:1055–1061.
52. Matsuzaki M, Ellis-Davies GC, Nemoto T, Miyashita Y, Iino M, Kasai H (2001): Dendritic spine geometry is critical for AMPA receptor expression in hippocampal CA1 pyramidal neurons. Nat Neurosci 4:1086–1092.
53. Kasai H, Ziv NE, Okazaki H, Yagishita S, Toyoizumi T (2021): Spine dynamics in the brain, mental disorders and artificial neural networks. Nat Rev Neurosci 22:407–422.
54. Holler S, Köstinger G, Martin KAC, Schuhknecht GFP, Stratford KJ (2021): Structure and function of a neocortical synapse. Nature 591:111–116.
55. McGlashan TH, Hoffman RE (2000): Schizophrenia as a disorder of developmentally reduced synaptic connectivity. Arch Gen Psychiatry 57:637–648.